World Weather Attribution

EMBARGO:

Thursday 12 December, 11am Eastern Time / 5pm Central European Time;

Friday 13 December, 12am (midnight) Philippines Time

Climate change supercharged late typhoon season in the Philippines, highlighting the need for resilience to consecutive events

Authors

Niklas Merz, *Centre for Environmental Policy, Imperial College, London, UK*
Ben Clarke, *Centre for Environmental Policy, Imperial College, London, UK*
Joseph Basconcillo, *Philippine Atmospheric, Geophysical and Astronomical Services Administration, Department of Science and Technology, Quezon City, Philippines*
Clair Barnes, *Centre for Environmental Policy, Imperial College, London, UK*
Nathan Sparks, *Department of Physics, Imperial College London, UK*
Maja Vahlberg, *Red Cross Red Crescent Climate Centre, The Hague, the Netherlands; Swedish Red Cross, Stockholm, Sweden (based in Ubmeje/Umeå, Sweden)*
Friederike Otto, *Centre for Environmental Policy, Imperial College, London, UK*

Review authors

Sjoukje Philip, *Royal Netherlands Meteorological Institute (KNMI), De Bilt, The Netherlands*
Sarah Kew, *Royal Netherlands Meteorological Institute (KNMI), De Bilt, The Netherlands*
Izidine Pinto, *Royal Netherlands Meteorological Institute (KNMI), De Bilt, The Netherlands*
Roop Singh, *Red Cross Red Crescent Climate Centre, The Hague, The Netherlands (based in New Jersey, USA)*
Afrhill Rances, *Asia-Pacific Regional Office, International Federation of Red Cross and Red Crescent Societies (IFRC), Kuala Lumpur, Malaysia*

Main findings

- The six consecutive typhoons that impacted northern Luzon between late October and November highlight the challenges of adapting to back-to-back extreme weather events. With 13 million people impacted and some areas hit at least three times, repeated storms have created a constant state of insecurity, worsening the region's vulnerability and exposure.
- The six typhoons impacted Luzon Island, which is comparably affluent, especially in the northern and central regions. Despite having the country's lowest household poverty rates, cities on the island remain highly vulnerable to flooding, particularly due to urban sprawl, river silting, and deforestation.
- To assess if human-induced climate change influenced the environmental conditions leading to the high number of storms, we first determine if there is a trend in the observation-based estimates of potential intensity. Our best estimate is that the observed potential intensity has become about 7 times more likely and the maximum intensity of a potential typhoon has increased by about 4 m/s (14.5 km/h).
- To quantify the role of human-induced climate change we also analyse climate models. The change in potential intensity attributable to human-induced climate change is smaller in the models than in the observations. When combining both, we find that the potential intensity as observed in 2024 has been made more likely by a factor of about 1.7, due to warming caused primarily by the burning of fossil fuels. The intensity has increased by about 2 m/s (7.2 km/h). These changes are projected to increase with further warming, meaning that in a 2.6°C warmer world the expected increase is another 2 m/s: this reflects projected conditions by the end of the century given currently implemented policies. As all models significantly underestimate the observed change, these numbers are assumed to be a conservative estimate of the role of climate change.
- Of the six major storms that affected the Philippines in late October-mid November 2024, three made landfall as major typhoons (defined as category 3 or above). We therefore also assess whether climate change has increased the odds of at least three major typhoons making landfall in the Philippines in a year. Using a statistical model we find that in today's climate, warmed by 1.3°C, such an event is expected once every 15 (6.5-45) years. That is 25% more frequent than it would have been had we not burned fossil fuels. In a 2°C warmer climate from pre-industrial times we expect at least 3 major typhoons hitting in a single year every 12 years (best estimate).
- For six storms to impact the northern Philippines in such a short period is extremely unusual, and it is difficult to study such an event directly because it is so rare. Overall, our results show that conditions conducive to the development of consecutive typhoons in this region have been enhanced by global warming, and the chance of multiple major typhoons making landfall will continue to increase as long as we continue to burn fossil fuels.
- The series of typhoons is one of several examples of consecutive events observed this year, for example floods in the Sahel Zone, and hurricanes Helene and Milton. Such consecutive extreme events make it difficult for populations to recover. Given the likelihood of compounding events will increase as the climate warms, it is crucial that communities take steps to become more resilient to extreme weather.
- The Philippines is advancing a proactive disaster risk management framework, highlighted by proposed legislation to formalize anticipatory action through a State of Imminent Disaster,

enabling preemptive resource allocation. This innovative approach complements robust emergency responses. However, consecutive typhoons have underscored the extraordinary challenge of ensuring continuity and resilience amidst escalating climate risks.

1 Introduction

On Saturday 16 November 2024, Super Typhoon Man-Yi made landfall in the Philippines with maximum sustained winds of 195 km/h. This event marks an unusually active month, being the 16th named storm of the annual season and the sixth typhoon to hit the Philippines within 30 days. Typically, November sees three named storms across the basin with one becoming a super typhoon, equivalent to a category 4 hurricane on the Saffir-Simpson scale, based on the 1991-2000 average (Nasa, 2024).

First, Tropical Storm Trami hit the northern Philippines at the end of October, killing more than a dozen people and dumping a month's worth of rain on the region. This was followed by Super Typhoon Kong-Rey, which killed at least three people and was described (BBC, 2024) as the biggest typhoon to hit Taiwan in around 30 years. The third typhoon in a month, Xinying, hit the island of Luzon in particular, forcing the evacuation of more than 160,000 people (The New York Times, 2024) with reported wind speeds of 240 km/h making it a super typhoon. The other two typhoons, Toraji and Super Typhoon Usagi, were accompanied by a three-metre storm surge and torrential rain (BBC, 2024; ACT Alliance, 2024). This sequence of storms hitting the Philippines followed Super Typhoon Krathon, which originated in the same area but made landfall in Taiwan in early October, causing numerous deaths and injuring more than 100 people. Furthermore, the Japan Meteorological Agency reported (CNN, 2024) that it was also the first time that four named storms had coexisted in the Pacific basin in November since records began in 1951. An overview of these storms, including the landfall date and categorisation is given in the table below.

Name (local name)	Landfall date	Type	Category (at landfall)
Krathon (Julian)	3rd October (Taiwan)	Super Typhoon	4
Trami (Kristine)	24th October (Philippines)	Typhoon	2
Kong-rey (Leon)	31rd October (Taiwan)	Super Typhoon	3
Yinxing (Marce)	7, November (Philippines)	Super Typhoon	4
Toraji (Nika)	11, November (Philippines)	Typhoon	1
Usagi (Ofel)	14, November (Philippines)	Super Typhoon	3
Man-yi (Pepito)	16, November (Philippines)	Super Typhoon	4

Table 1.1: *Overview of the seven named typhoons in the study area between September and November. The classification at landfall is based on the Saffir-Simpson scale, while the type description is based on the typhoon's peak wind speed.*

The compounding impacts of this sequence of storms resulted in devastating damages to the infrastructure. Early estimates are around the order of 430 million USD (NDRRMC, 2024) for the seven named storms above, including damages to houses, infrastructure and agriculture. The storms Trami and Kong-Rey alone killed more than 160 people, displaced more than 600,000 people from their homes and affected around 9 million individuals across the whole region (ACT Alliance, 2024). Collectively, these numbers rise to more than 13 million affected people in 17 out of 18 of Philippines' 18 regions and displacing more than 1.4 million people (OCHA, 2024).

In the western North Pacific basin, the more active cyclone season runs from June to November. In the later half of the season, from September to November (SON), a sequence of strong storms all affected a very similar region around the northern Philippines. This was driven by a combination of factors. First, there was an extremely high intensity of the Western North Pacific Subtropical High (WNPSH), which influenced the surrounding weather patterns (Figure 1.1a, c). When the WNPSH is farther north, as it was during SON 2024, tropical cyclones (TCs) are steered around its southern flanks, resulting in more TCs heading towards the Philippines. In addition, since mid-April 2024, there has been persistently high ocean heat content in the TC genesis area in the Philippine Sea (NOAA, 2024). In SON 2024 in particular, the 20°C isotherms have been warmer and deeper than unusual (Figure 1.1b), indicating that the upper ocean holds more heat than usual, providing a continuous source of fuel for TC genesis and intensification. As the warm water penetrates deeper into the ocean, there is an expected stronger ocean stratification resulting in a reduced or contained upwelling of colder waters to the surface layers. TCs that pass through areas with reduced upwelling are more likely to maintain their intensity or intensify. This is evident in Figure 1.1b, where the cold wake associated with the TC passages in SON 2024 is mostly contained along the TC tracks in Figure 1.1a. The combination of these factors created favourable conditions for frequent and intense tropical cyclones.

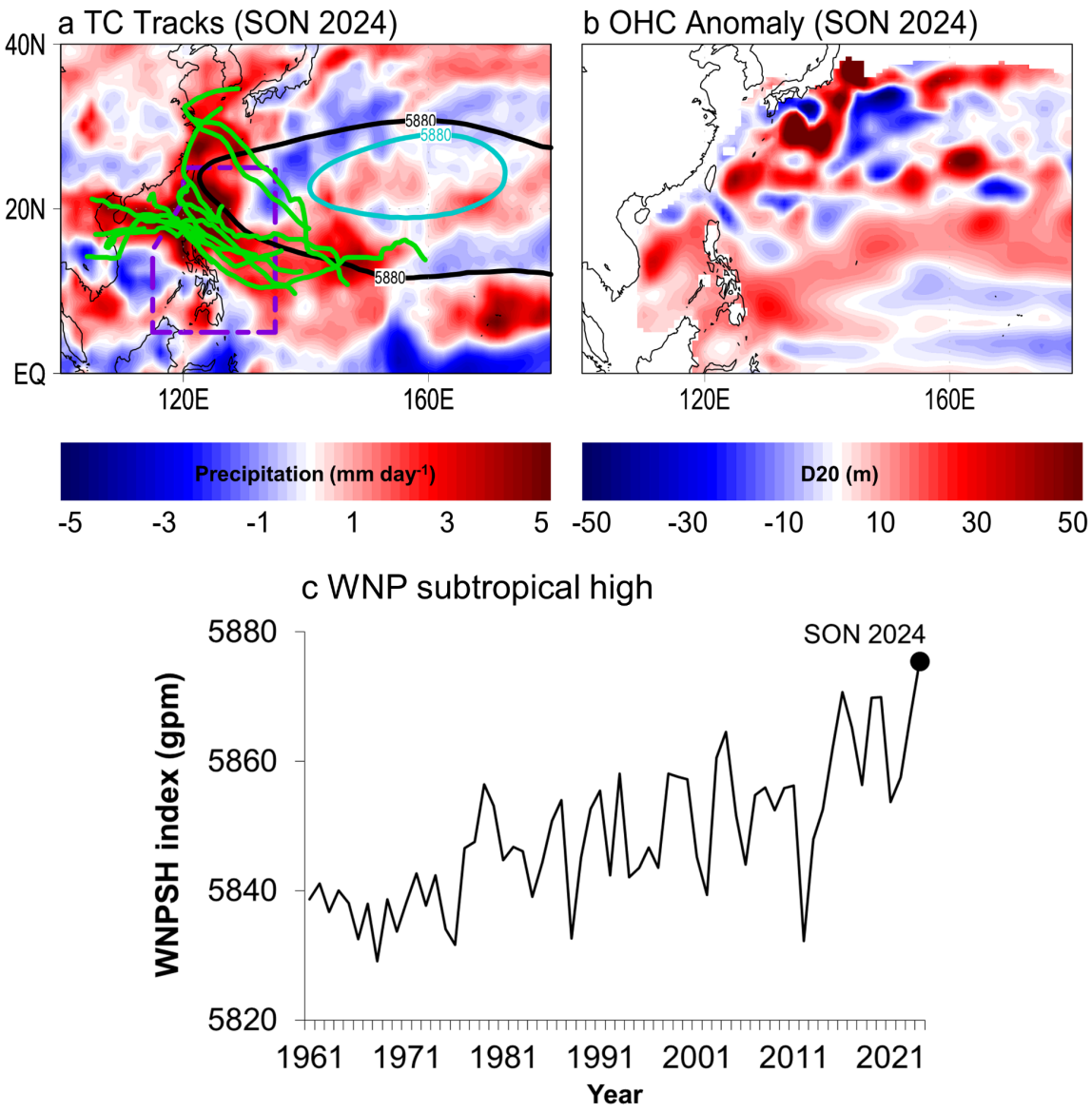

Figure 1.1: *(a) Tracks of tropical cyclones (TC, solid green line) that crossed the Philippine Area of Responsibility (dashed purple line) in September-November (SON) 2024. The location of the Western North Pacific subtropical high (WNPSH) is shown using cyan (1991-2020 climatology) and black lines (SON 2024), respectively. (b) Anomaly in the depth of the 20°C isotherms. Positive anomalies indicate deeper isotherms compared to the climatology. (c) Time series of the WNPSH index during SON from 1961-2024. Atmospheric and ocean reanalysis data are obtained from the JRA-3Q and the MOVE-G3 while the best TC track data is from the IBTrACS.*

1.1 Typhoons in the Western North Pacific and climate change

The Western North Pacific basin (WNP) is the most active TC region globally (Wang & Wang, 2023), exposing nations across east and southeast Asia to extreme weather conditions. The Philippines is one of the nations most affected by TCs in the world, with approximately 19 TCs in the Philippines area

of responsibility and on average 9 landfalls per year (Santos, 2020; Cinco et al., 2016). The majority of TCs occur during the most active months of June-November, with a less active season from December-March, though events have historically occurred at all times of the year (Basconcillo & Moon, 2021; Basconcillo et al., 2024).

Globally, the overall frequency of tropical cyclones is not significantly changing in time, but there is evidence that the most intense TCs (categories 3-5 on the Saffir-Sampson hurricane wind scale) are increasing in number (Knutson et al., 2021). This is in part due to increased sea surface temperatures (SSTs). Additionally, rainfall from TCs is becoming more intense in part due to the Clausius-Clapeyron relation, which states that warmer air holds more moisture at a rate of 6-7% / °C.

On the scale of individual basins, more complex changes are emerging. In the WNP, there may have been a slowdown in translation speed (the horizontal movement of a TC) (Lai et al., 2019; Yamaguchi and Maeda, 2020a), as well as a poleward (northward) shift in storm tracks (Yamaguchi and Maeda, 2020b; Kossin et al., 2016). In the Philippines, no trend in landfalling rate has been found to date (Cinco et al., 2016). Changes are also occurring at sub-basin scales. For instance, in Southeast (East) Asia, there is evidence of a decreasing (increasing) trend in TC passages during the boreal autumn (around September-October), which is linked to decadal-scale variability (Basconcillo and Moon, 2023). Coupled to this, analysis of annual mean accumulated cyclone energy (ACE) in the Philippines' area of responsibility has seen an abrupt increase since 2003 (Basconcillo et al., 2022).

Attribution studies help to elucidate the emerging impact of human induced warming on TCs in the basin. In the Philippines, a study using a Pseudo-Global warming approach showed that the wind speeds associated with landfalling typhoons Bopha, Mangkhut and Haiyan were, respectively, 10 m/s, 2 m/s and 2 m/s higher than they would have been in a preindustrial climate (Delfino et al., 2023). Another study found that the storm surge from Haiyan was 20% higher due to human-induced warming (Takayabu et al., 2015). In Japan, the extreme rainfall associated with typhoon Hagibis in 2019 was found to be 15-150% more likely to occur because of human induced warming, which in turn was linked with an increase of approximately US$4 billion in damages (Li & Otto, 2022). In addition, a storyline-based attribution study found that rainfall from the typhoon was amplified by around 11% due to human-induced warming across the atmosphere and oceans (Kawase et al., 2021). Similarly, in early August 2009, Typhoon Morakot made landfall and stalled in Taiwan, causing extreme rainfall. The previous 20 years of anthropogenic forcing were found to account for an increase of approximately 3.5% in the rainfall total (Wang et al., 2019). Finally, in 2020, central Vietnam experienced a series of typhoon-induced extreme rainfall events leading to severe impacts, but a study found that anthropogenic climate change had no detectable influence on the rainfall from the consecutive events when they struck Vietnam (Luu et al., 2021).

Studying the anthropogenic influence on individual tropical cyclones is challenging for several reasons. First, observation records predating the satellite era are very sparse (Walsh et al., 2016). Second, there are many conditions and physical mechanisms through which climate change may affect the impact of a given storm or storm season, such as sea surface temperatures, sea level, vertical wind shear, genesis location, steering pattern, and intensification rate, among others (Knutson et al., 2021). Finally, the extreme winds are the result of phenomena at scales on the order of ~10 km or less, meaning that almost all climate models cannot resolve the most extreme events and higher-resolution bespoke modelling is required to explicitly simulate them (Wehner et al., 2019). The timescale of rapid attribution makes this even more challenging, as it is not possible to set up and validate higher

resolution models. To date, most rapid studies have been conducted only for rainfall totals over relatively large areas that can be reasonably captured by climate models at resolutions of ~25-50 km, including Hurricanes Harvey (van Oldenborgh et al., 2017) and Imelda (van Oldenborgh et al., 2019), ex-TC Gabrielle in New Zealand (Harrington et al., 2023), and a series of cyclones affecting Mozambique (Otto et al., 2022). Recent rapid attribution studies for Hurricane Helene and Typhoon Gaemi have evaluated the anthropogenic influence on several variables such as rainfall, wind and the conditions leading up to such an event, all of which are important aspects of the impact of such storms. In this study, we aim to assess whether and to what degree climate change influenced conditions conducive to the formation of TCs, and the likelihood of observing a sequence of TCs like the one that affected the Northern Philippines in November 2024. Individual event definitions are given in sections 2 and 3.

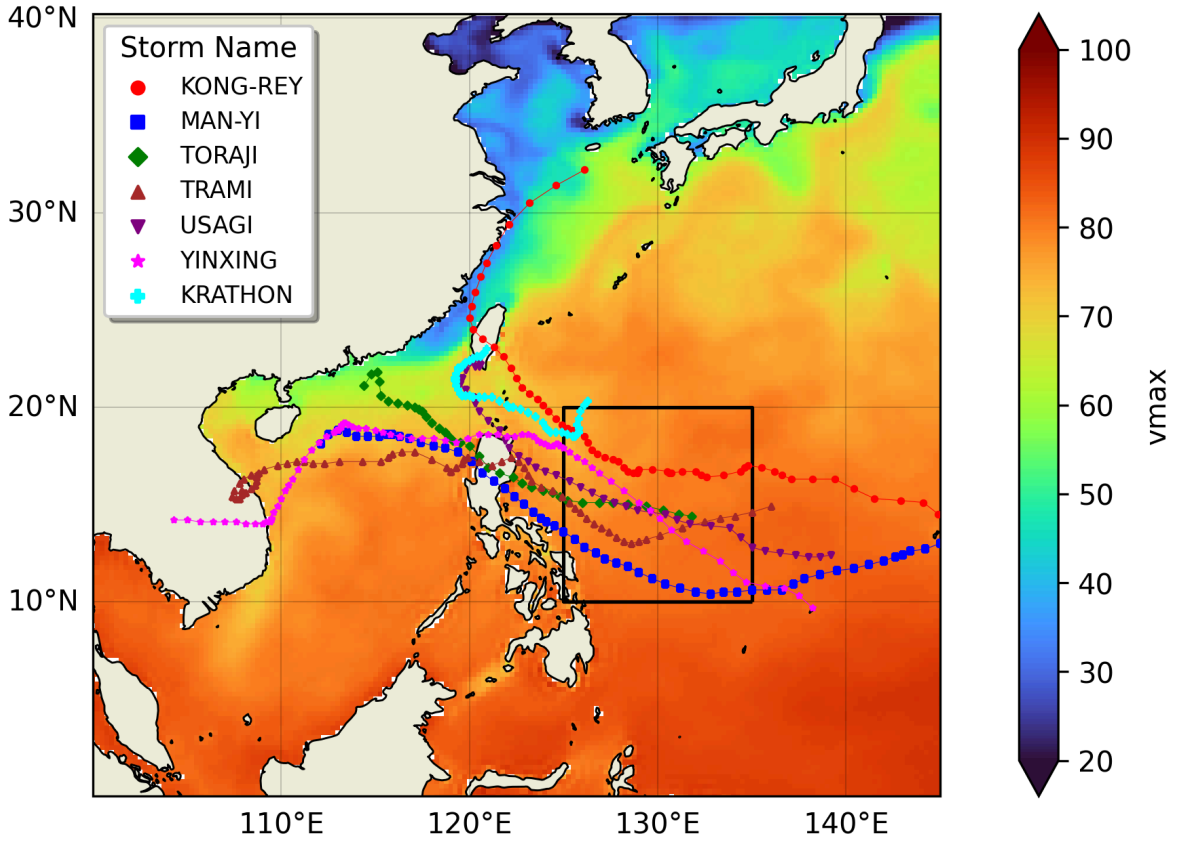

Figure 1.2: *Mean potential intensity (m/s) in the Philippine Sea during Sep-Nov 2024. The study region is indicated by a black box and the tracks of storms during this time are shown as points in different colors. Data from ERA5.*

2 Potential Intensity attribution using WWA protocol

The event definition studied in this section is as follows:

- **Potential intensity (PI):** September-November monthly max PI over an ocean area bounded by 125-135 °E, 10-20 °N (Figure 1.2).

We evaluate the influence of anthropogenic climate change by comparing the likelihood and intensity of similar PI conditions to those observed in 2024 with what would be expected in a 1.3 °C cooler climate. We also extend the analysis into the future by assessing the influence of a further 1.3 °C of global warming from present: this reflects projected conditions by the end of the century given currently implemented policies (UNEP, 2024).

2.1 Data and methods

2.1.1 Observational data

Two reanalysis datasets are used in this study to calculate the PI:

- The European Centre for Medium-Range Weather Forecasts's 5th generation reanalysis product, ERA5, starting from 1940 at 0.25° horizontal resolution (Hersbach et al., 2020).
- The Modern-Era Retrospective analysis for Research and Applications version 2, MERRA2, is used as a second observation-based dataset (Gelaro et al., 2017). It is a gridded dataset covering the satellite observation era from 1980 to the present at 0.625 by 0.5° horizontal resolution.

Finally, as a measure of anthropogenic climate change we use the (low-pass filtered) global mean surface temperature (GMST), where GMST is taken from the National Aeronautics and Space Administration (NASA) Goddard Institute for Space Science (GISS) surface temperature analysis (GISTEMP; Hansen et al., 2010 and Lenssen et al. 2019).

2.1.2 Model and experiment descriptions

To estimate the influence of anthropogenic climate change upon the potential intensity in which this sequence of typhoons occurred, we use monthly data from the CMIP6 multi-model ensemble. This consists of simulations from multiple participating models with varying resolutions. For more details on CMIP6, see Eyring et al., (2016). For all simulations, the period 1850 to 2015 is based on historical simulations, while the SSP5-8.5 scenario is used for the remainder of the 21st century. A single realization is used for each of the CMIP6 models.

2.1.3 Calculation of the potential intensity

The potential intensity is calculated from sea surface temperatures, sea level pressure, and temperature and humidity at all pressure levels using the open-source PyPI package (Gilford, 2021) following the methods laid out in Pérez-Alarcón et al., 2023 and Emanuel, 1986.

2.1.4 Statistical methods

The methods for attribution are set out in detail in appendix section A.1. In summary, a nonstationary Gaussian distribution is used to model PI, and the distribution is assumed to shift linearly with the covariate GMST, while the variance remains constant.

2.2 Observational analysis: trend and return period

Figure 2.1 shows the time series of maximum monthly PI from September-November, calculated from ERA5 (panel a-b) and MERRA-2 (panels c-d), along with the fitted statistical model described in Section 2.1.4. Panels a and c show the fitted mean trend (black line) along with the estimated return levels of 6-year and 40-year events (blue lines). The PI index exhibits a strong and statistically significant increasing trend with warming for ERA5, implying that the maximum wind speed has increased by about 4 m/s. In MERRA-2 the trend is of similar magnitude, but the uncertainty is somewhat higher and so the increase is not found to be statistically significant (Table 1.2). In both datasets, the PI in the region of the September-November typhoons has a return period of approximately 2 years in the present climate. In both datasets the probability of experiencing SON maximum monthly PI as high as that recorded in 2024, has become around seven times more likely due to 1.3 °C of warming (panels b and d); this means that, in a climate without human induced warming, the event would have a return period of approximately 15 years.

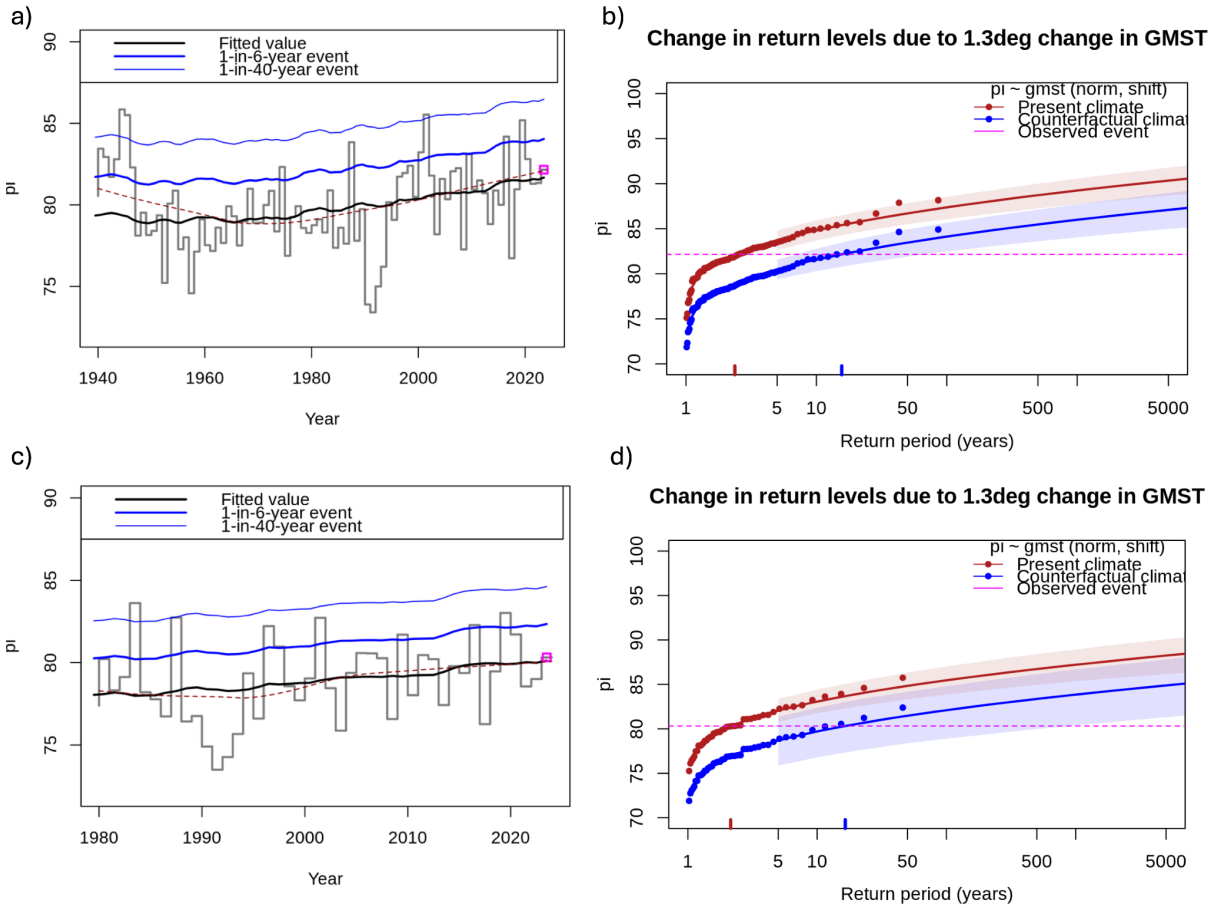

Figure 2.1: *(a, c) Time series of max monthly September-November potential intensity, averaged over the study region, in ERA5 (top) and MERRA2 (lower). The heavy black line indicates the mean of the nonstationary distribution in each year, with the 6-year and 40-year effective return levels in blue. The dashed red line is a nonparametric Loess smoother; the pink square marks the 2024 total. (b, d) Expected return levels for SON maximum PI over the study region at the 2024 GMST (red lines) and 1.3°C lower GMST (blue line), estimated from the statistical model. Shaded regions represent 95% confidence intervals obtained via a bootstrapping procedure. The dashed pink line indicates the observed PI.*

Dataset	Return period	Probability Ratio	Change in magnitude (m/s)
ERA5	2.4 (1.6 ... 3.8)	6.6 (2.2 ... 34)	4.1 (1.8 ... 6.6)
MERRA2	2.1 (1.4 ... 3.7)	7.7 (0.88 ... 6.2e+2)	4.4 (-0.24 ... 9.8)

Table 2.1: *Return period, change in probability ratio and magnitude for the potential intensity in September-November 2024 in the studied region due to GMST. Dark (light) blue indicates a statistically (non)significant increasing trend.*

2.3 Model evaluation

In the subsections below we show the results of the model evaluation for the assessed region (individual figures shown in appendix A.2). The climate models are evaluated against the observations in their ability to capture:

1. Seasonal cycles: For this, we qualitatively compare the seasonal cycle of PI based on model outputs against observations-based cycles. We discard any models that exhibit ill-defined peaks in their seasonal cycles.

2. Spatial patterns: Models that do not match the observations in terms of the large-scale spatial pattern of SON mean PI are excluded.

3. Fit Quality: We evaluate the fitted statistical models by qualitatively assessing whether the fitted normal distribution matches the data points. If the PI data values (data points) are not close to the expected PI (lines) then the chosen statistical distribution is not a good fit to the model data, and the model is discarded.

We note that in almost all of the climate models evaluated, the standard deviation of the fitted model was somewhat higher in the climate model than in the reanalyses, implying a systematic bias. We therefore only evaluate the fit of the statistical model, rather than comparing the scale parameters of the models as in the standard WWA protocol.

The models are labelled as ‘good’,’reasonable’, or ’bad’ based on their performances in terms of the three criteria discussed above. A model is given an overall rating of ‘good’ if it is rated ‘good’ for all three characteristics. If there is at least one ‘reasonable’, then its overall rating will be ‘reasonable’ and ‘bad’ if there is at least one ‘bad’.

Of the 19 CMIP6 models analysed, 8 were rated ‘bad’ and discarded from the attribution analysis. Only one model performed well across all criteria, so all 11 ‘good’ or ‘reasonable’ models were used.

Model / Observations	**Seasonal cycle**	**Spatial pattern**	**Fit Quality**	**Sigma**	**Conclusion***
ERA5				2.45 (1.99 ... 2.81)	
MERRA2				2.29 (1.80 ... 2.69)	
CMIP6					
ACCESS-CM2 (1)	reasonable	good	reasonable	4.59 (3.79 ... 5.22)	reasonable
BCC-CSM2-MR (1)	reasonable	good	good	3.98 (3.27 ... 4.52)	reasonable
CanESM5 (1)	good	good	good	3.32 (2.65 ... 3.88)	good
CanESM5-CanOE(1)	good	reasonable	reasonable	3.34 (2.84 ... 3.78)	reasonable
CMCC-CM2-SR5 (1)	good	good	bad	5.64 (4.73 ... 6.31)	bad
CMCC-ESM2 (1)	good	good	reasonable	5.43 (4.61 ... 6.02)	reasonable
E3SM-1-1 (1)	reasonable	good	bad	5.27 (4.50 ... 5.89)	bad
HadGEM3-GC31(1)	good	reasonable	good	3.96 (3.41 ... 4.40)	reasonable
INM-CM5-0 (1)	reasonable	reasonable	good	2.03 (1.52 ... 2.45)	reasonable
KACE-1-0-G (1)	bad	reasonable	bad	5.33 (4.51 ... 6.01)	bad
KIOST-ESM (1)	reasonable	reasonable	reasonable	3.38 (2.88 ... 3.81)	reasonable
MIROC-ES2L (1)	bad	reasonable	good	4.16 (3.45 ... 4.71)	bad
MIROC6 (1)	reasonable	reasonable	bad	4.85 (3.97 ... 5.59)	bad
MPI-ESM1-2-LR (1)	reasonable	good	reasonable	5.60 (4.57 ... 6.45)	reasonable
NESM3 (1)	reasonable	reasonable	reasonable	4.79 (3.81 ... 5.58)	reasonable
NorESM2-LM (1)	reasonable	good	bad	5.39 (4.55 ... 6.08)	bad
NorESM2-MM (1)	reasonable	good	bad	5.12 (4.27 ... 5.77)	bad
TaiESM1 (1)	reasonable	reasonable	bad	6.73 (5.87 ... 7.41)	bad
UKESM1-0-LL (1)	good	reasonable	reasonable	4.29 (3.72 ... 4.78)	reasonable

Table 2.3: *Evaluation of the climate models considered for attribution of potential intensity for the studied region. For each model, the best estimate of the standard deviation parameter (sigma) is shown with a 95% confidence interval obtained via bootstrapping. The overall evaluation is shown in the right-hand column. The conclusion is based on the seasonal cycle, spatial pattern and fit quality.*

2.4 Multi-method multi-model attribution

This section shows Probability Ratios and change in intensity ΔI for models that passed model evaluation and also includes the values calculated from the fits with observations. A description of how to interpret these figures can be found in Appendix A.3.

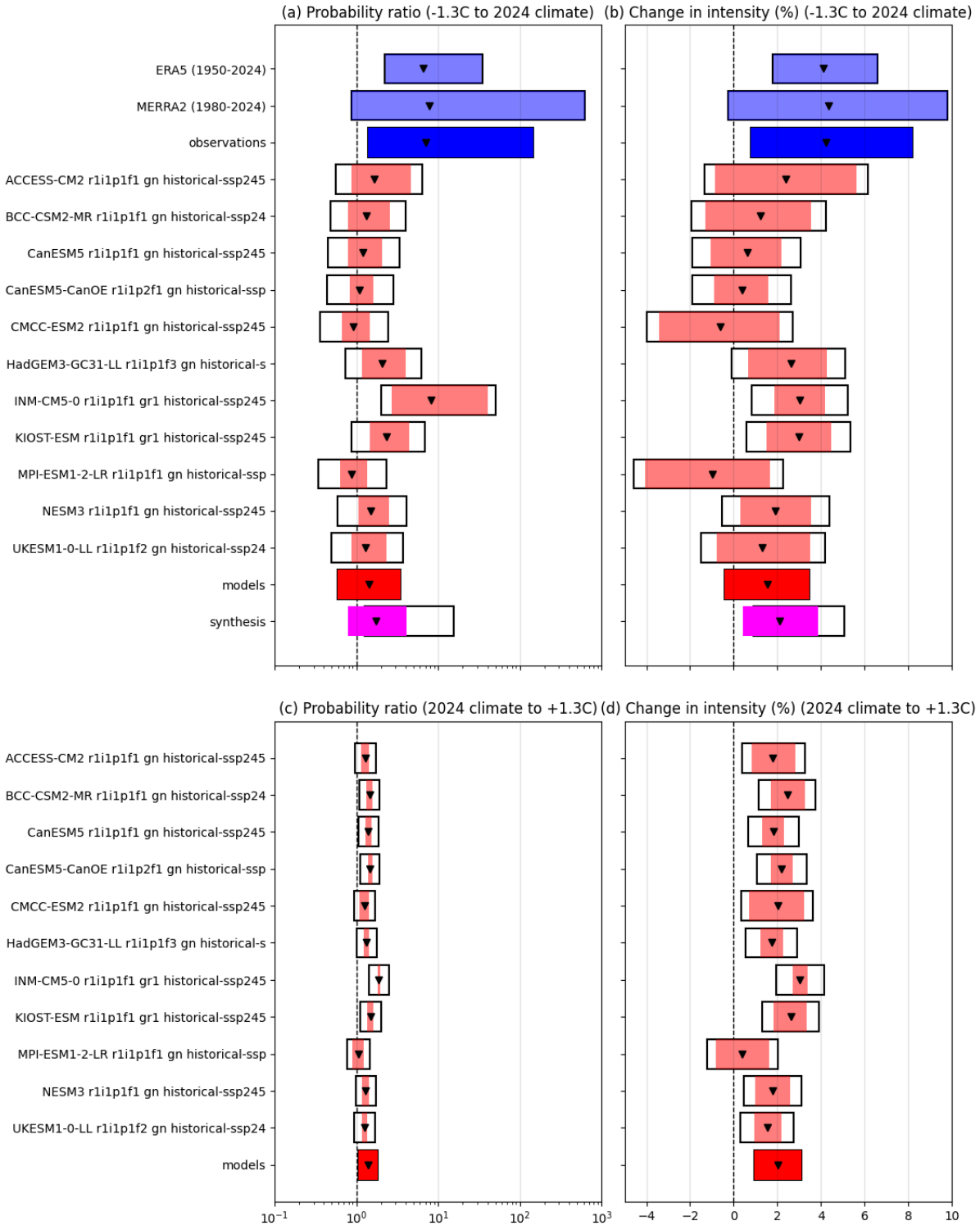

Figure 2.2: *Synthesised changes for SON maximum potential intensity in the study region. Changes in PR (left) and intensity (right) are shown for a historical period comparing the past 1.3 °C cooler climate with the present (top row) and for a future period, based on model projections only, comparing the present and a 2.6 °C warmed climate (bottom row).*

3 Landfall rate attribution using IRIS

The event definition studied in this section is as follows:

- **Multiple Philippines landfalls:** number of typhoons at or above category 3 (defined as wind speeds of at least 50 m/s) making landfall in the Philippines each year

Given the infrequency of landfalling tropical cyclones (TC) and the short period of reliable observations, assessing tropical cyclone risk remains a challenge. Synthetic tropical cyclone datasets can help overcome these problems. We explore this approach here using a new global tropical cyclone wind model (IRIS) with several key innovations (Sparks and Toumi, 2024). It recognises that the key step for estimating landfall wind speed is the location and value of the lifetime maximum intensity (LMI) and redefines the problem as one of decay only. The lifetime maximum intensity is assumed to be physically constrained by the thermodynamic state as defined by the potential intensity (PI).

In this section we analyse the change in likelihood of at least 3 TCs of at least category 3 making landfall in the Philippines in a given year. To avoid counting multiple landfalls from a single storm passing over the archipelago, the analysis uses only one landfall (the landfall with highest landfall intensity) per storm. While these results are for the entire nation, they are likely to be representative of the change in likelihood for the northern island only, given that the majority of TCs affect that region.

3.1 Data and methods

Observed 'parent' tracks from the IBTrACS database, truncated to begin at the location at which the LMI occurs, are perturbed to create synthetic 'child' tracks. Observations show that the relative intensity along a TC's track, defined as observed maximum intensity divided by the potential intensity, follows a robust uniform distribution; this is used to derive a stochastic model for the lifetime maximum intensity of the 'child' tracks, which is then assumed to decay stochastically over time, with different rates of decay over sea and land surfaces. In this way, extremely large synthetic datasets of realistic storm tracks can be generated at relatively low computational cost, sampling the landfall intensity and location. The simulation approach is described in detail in (Sparks and Toumi, 2024).

Regional and local prediction of absolute PI by climate models is problematic as they are known to have biases. We therefore use the observed PI trend since 1979 from ERA-5; to estimate the pre-industrial (future) potential intensity state we extrapolate backwards (forwards) the current observed trends to a climate that is 1.3 °C cooler than now (0.7 °C warmer than now). Because regional observed changes are difficult to distinguish from natural variability we make the assumption that the anthropogenic trend is the global zonal mean PI trend. This method is simple and robust, and avoids the need to bias-correct climate models to estimate trends in PI.

3.2 Attribution

We evaluated the change in occurrence of at least three major typhoons (category 3 or above) making landfall in the Philippines in a given year. In the present climate, such an event occurs roughly once every 15 (6.5-45) years, but prior to warming of 1.3 °C would have occurred only once every 19 years (Figure 3.1). This represents an increase in likelihood of approximately 25%; alternatively, 20% of occurrences of 3 or more TCs making landfall in the Philippines in a single year can be attributed to this warming. In the future at 2 °C of warming - a further 0.7 °C from present day - such events are expected to occur every 12-13 years. This represents a further increase of around 21% in likelihood.

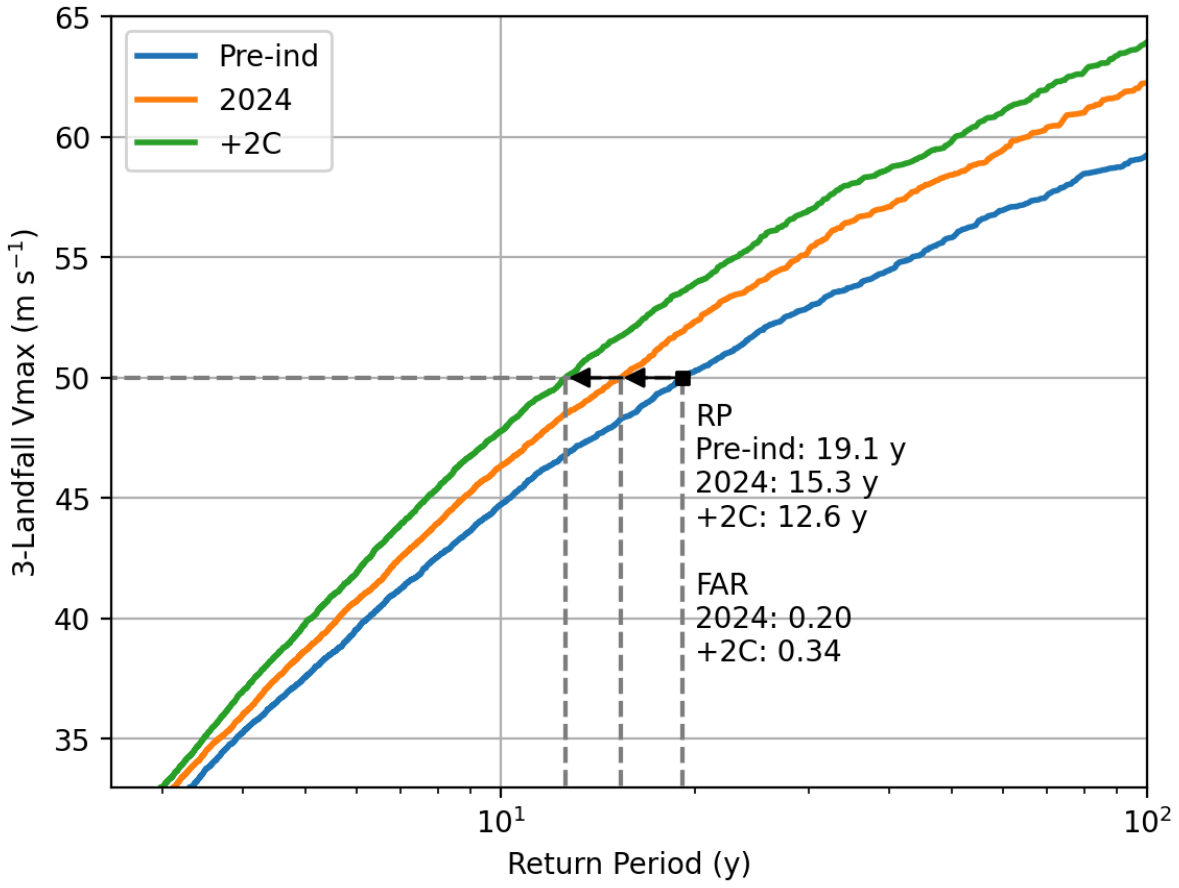

Figure 3.1: *Return level curves for tropical cyclones making landfall in the Philippines. The orange curves show the present day climate in 2024, while the blue curves show the pre-industrial climate and green shows the future 2 degrees warmer world.*

4 Hazard summary

This section contains all of the final results for each hazard analysis.

Changes in the maximum SON monthly potential intensity are shown in table 4.1. Models and observations strongly agree that the PI has increased in line with GMST. The observation-based reanalysis gives a strong and significant trend, with a probability ratio (PR) of 7.13 (95% confidence interval: 1.38-147) and a change in intensity of 4.24 (0.78-8.2) m/s. The trend in the models is smaller and not significant, but the four models that simulate a significant change in PI in response to global warming all simulate an increase, and five of the remaining models also agree on the sign of the change. The general model change is in the same direction as in observations, which suggests that the model results at least qualitatively represent the climate change signal well; however, given that almost all of the models overestimate the variability of PI, we note that they may not accurately represent the strength of the trend.

Synthesising both data sources, we find that such conditions have become more likely by a factor of 1.74 (0.78-4.15) and significantly more intense with a change of 2.12 (0.41-387) m/s. We used the weighted uncertainty range (magenta bar in Figure. 2.2) as the model best estimate is within the observed uncertainty; however, as all models significantly underestimate the observed change, these numbers are probably a conservative estimate of the role of climate change. For the future, the models project a significant increase in the likelihood, with strong agreement between all 11 models (Figure 2.1). The projected increase in intensity is 2.02 (0.95-3.09) m/s, which is approximately again the increase between pre-industrial levels and today.

Finally, using IRIS, we find that the likelihood of 3 or more major typhoons (defined as category 3 or above) making landfall in the Philippines, as occurred in 2024, has increased by approximately 25% (from a one in 19.1 year event to a one in 15.3 year event), a result that is consistent with the synthesised probability ratio for the PI. The results for the landfall of a single major typhoon (shown in appendix A.4) show an increased likelihood of approximately 13% due to current warming (summarised in table 4.2). This in turn underscores the increased risk in a warming climate of compounding events like the sequence of TCs that affected Luzon in 2024; while individual TCs have increased in likelihood and intensity, the risk of multiple such storms affecting the Philippines in rapid succession has increased twice as much. We acknowledge that this result is based on one stochastic model with a limited analysis of the associated uncertainties, but also underline that it is in agreement with other multi-model analysis of PI conditions.

Data		**Potential intensity**	
		Probability ratio	**Change in intensity (m/s)**
Observations	**Past - present**	7.13 (1.38 … 147)	4.24 (0.775 … 8.20)
Models		1.42 (0.585 … 3.46)	1.53 (-0.426 … 3.48)
Synthesis		1.74 (0.781 … 4.15)	2.12 (0.412 … 3.87)
Models only	**Present - future**	1.38 (1.05 … 1.82)	2.02 (0.950 … 3.09)

Table 4.1: *Summary of results for changes in SON maximum monthly potential intensity in the study region shown in Figure 2.2. Statistically significant increases in probability and intensity are highlighted in dark blue, while non-significant increases are highlighted in light blue.*

Annual number of landfalling major typhoons	**Return period (years)**		**Probability ratio**
	Preindustrial	**Current conditions**	
3+	19.1	15.3	1.25
1+	1.21	1.07	1.13

Table 4.2: Changes in landfall rate of major typhoons for the Philippines in current and preindustrial conditions.

For six storms to impact the northern Philippines in such a short period is extremely unusual, and it is difficult to study such an event because it is so rare. Overall, our results show that the rate of landfalling major TCs and the conditions leading to the high number of TCs during SON in the study area (125-135°E, 10-20°N) have all increased due to climate change. In particular, winds have become more likely and more intense, the likelihood of subsequent storms making landfall in the Philippines has increased, and the potential intensity conditions leading to such events have become and will continue to become more intense. It is therefore also overwhelmingly likely that the impacts of the TCs during SON 2024 were more severe as a result of climate change. These impacts, and the future risk of similar impacts, are also directly related to the multiple aspects of vulnerability and exposure of people affected by such compounding storms (see section 5).

5 Vulnerability and exposure

Between mid-October and November of 2024, an unprecedented series of six consecutive typhoons affected the northern and central regions of Luzon Island. Despite its relative affluence and being home to the country's ten cities with the lowest household poverty rates (Berse, 2022), Luzon still has pockets of vulnerability. Provincial cities in northeastern Luzon, such as Ilagan, Tuguegarao, Santiago and Cauayan, face increased flood risk due to several environmental and anthropogenic factors. Key drivers of this include urban sprawl, river silting, and deforestation, particularly in Central Luzon (National Economic and Development Authority Regional Office, 2017; Alecha et al., 2022; Mata et al., 2022). Deforestation exacerbates the risk by reducing the watershed's ability to absorb and slow down rainfall, while river silting increases water levels during heavy rainfall, further raising the flood risk. Furthermore, as highlighted by recent studies on Tuguegarao City, population density is a key factor, as more densely populated areas near rivers face greater vulnerability (Alecha et al., 2022).

Further, the cities in northern Luzon are also highly exposed due to their geographical setting (Mata et al., 2022). The low-lying Cagayan Valley, for example, is a natural catch basin for floodwaters from surrounding tributaries, with Tuguegarao situated close to two major rivers, making it particularly susceptible to inundation during the peak typhoon season and monsoon.

Rural communities, particularly in the Cagayan Valley, are highly vulnerable to weather shocks due to their dependence on climate-sensitive livelihoods, with agriculture serving as the main economic driver in provinces like Cagayan and Isabela (Department of Agriculture, 2019; Philippine Statistics Authority, 2024; Provincial Government of Cagayan, n.d.). The typhoons have severely impacted Luzon's agricultural output, with critical losses in key crops like rice, corn, and vegetables (GMA, 2024) which exceed USD 23 million in Cagayan alone (Fresh Plaza, 2024). During the main rice planting season, typhoons disrupt planting or delay harvesting, leading to the risk of immediate food shortages and higher prices, such as a 10-15% surge in vegetable prices (Business World, 2024). These compounding shocks hamper recovery, elevating long-term risks to food supply (especially as they hit during the lean harvesting season) (IFRC, 2024) and prolonging food insecurity, which is already third-highest in Southeast Asia at 44.1% of the population (FAO et al., 2024). Disruptions affect both local food availability and national exports, weakening the country's position in global markets and posing a significant economic strain.

In the Philippines, there is growing recognition of the need to advance integrated climate and disaster risk governance as a means to better prepare for and respond to climate-related risks. Recently, the country proposed a bill to establish a State of Imminent Disaster, which would formalize and implement anticipatory action within governmental frameworks. This proposed legislation, which would be the first of its kind globally, aims to enable the allocation of national and local resources to take preventive measures prior to the occurrence of a predicted disaster (Anticipation Hub, 2024; IFRC Disaster Law, 2021).

The Philippine Red Cross' (PRC) operational strategies for emergency response were characterized by rapid deployment of resources, coordination with governmental bodies, and adaptive revisions to emergency appeals to address the escalating impacts. The PRC leveraged thousands of volunteers for immediate disaster relief. Emergency services prioritized Water, Sanitation, and Hygiene (WaSH), debris clearance, and distribution of hot meals (IFRC, 2024).

While disaster risk reduction, adaptation and emergency response strategies are essential, the scale and frequency of these events render these measures inadequate. The series of six consecutive typhoons that impacted northern Luzon between late October and November, in particular, illustrates potential limits to adaptation in the face of repeated extreme weather events. Aggravating vulnerabilities in shelter, health and livelihood sectors (IFRC, 2024), repeated typhoons lead to a perpetual state of insecurity, with 13 million people affected and certain areas affected at least three times (OCHA, 2024). Many communities remained evacuated between typhoons for extended periods of time. Families reliant on subsistence agriculture face relentless crop and livelihood losses, leaving millions with disrupted income, and at increased risk of food insecurity and debt (UN DESA, 2024). Housing, at times hastily reconstructed with substandard materials (UNISDR, 2019; Cajilig et al., 2023; Cervantes, 2017), is more easily destroyed by subsequent typhoons. Psychological stress also intensifies as individuals experience extreme weather events, including recurring trauma, compromising their capacity to recover (Alibudbud, 2023; Aruta et al., 2022; Aruta & Simon, 2022).

On a systemic level, the repeated typhoons expose weaknesses in infrastructure. Roads, bridges, and flood defenses, if not already compromised by earlier storms, become even more vulnerable with each passing typhoon, eroding development gains (Schleypen, Plinke & Geiger, 2024). With extensive damage to transportation, power, and communication systems hindering the distribution of aid, and infrastructure damages preventing public access to utilities, healthcare, and education, the government faced challenges in rolling out relief and responding to needs (IFRC, 2024). This led to prolonged recovery times and reduced community resilience (Schleypen, Plinke & Geiger, 2024).

The compounding effects of these typhoons also erode coping capacities at household level, as families' ability to recover is overwhelmed by the frequency of losses and the lack of time to rebuild. Often, households are forced to employ erosive coping strategies which negatively impact their long-term livelihoods and resilience, such as selling assets, reducing food consumption, and contracting debts (IOM, n.d.; Israel & Briones, 2014).

Resilience-building efforts are critical, but these must be complemented by systemic, global measures to mitigate climate change. Without transformative changes, Luzon's vulnerabilities are likely to deepen, leaving affected populations trapped in a cycle of destruction and recovery. Transformative changes involve addressing the root causes of vulnerability while enhancing the capacity of communities to withstand and recover from shocks such as weather-related disasters. Specifically, this can entail reforesting degraded areas and protecting watersheds, investing in resilient infrastructure such as elevated roads and decentralized power systems, promoting climate-smart agriculture and crop diversification, and finalizing the State of Imminent Disaster bill to further the paradigm shift towards anticipatory action.

Data availability

All time series used in the attribution analysis are available via the Climate Explorer.

References

All references are given as hyperlinks in the text.

Appendix

A.1 Statistical methods

Methods for observational and model analysis and for model evaluation and synthesis are used according to the World Weather Attribution Protocol, described in Philip et al., (2020), with supporting details found in van Oldenborgh et al., (2021), Ciavarella et al., (2021) and here. The key steps, presented in sections 3-6, are: (3) trend estimation from observations; (4) model validation; (5) multi-method multi-model attribution; and (6) synthesis of the attribution statement.

In this report we analyse time series representing the maximum monthly Potential Intensity value during the time period from September to November each year for different reanalysis and model datasets. A nonstationary Gaussian distribution is used to model this variable. As the Potential Intensity is largely driven by the Sea Surface Temperature (SST), the distribution is assumed to shift linearly with the covariates, while the variance remains constant. The parameters of the statistical model are estimated using maximum likelihood.

For each time series we calculate the return period and intensity of the event under study for the 2024 GMST and for 1.3 °C cooler GMST: this allows us to compare the climate of now and of the preindustrial past (1850-1900, based on the Global Warming Index), by calculating the probability ratio (PR; the factor-change in the event's probability) and change in intensity of the event. We also repeat the calculations using a 1.3 °C warmer GMST, allowing us to quantify the changes in a hypothetical future world of continued warming.

A.2 Model evaluation

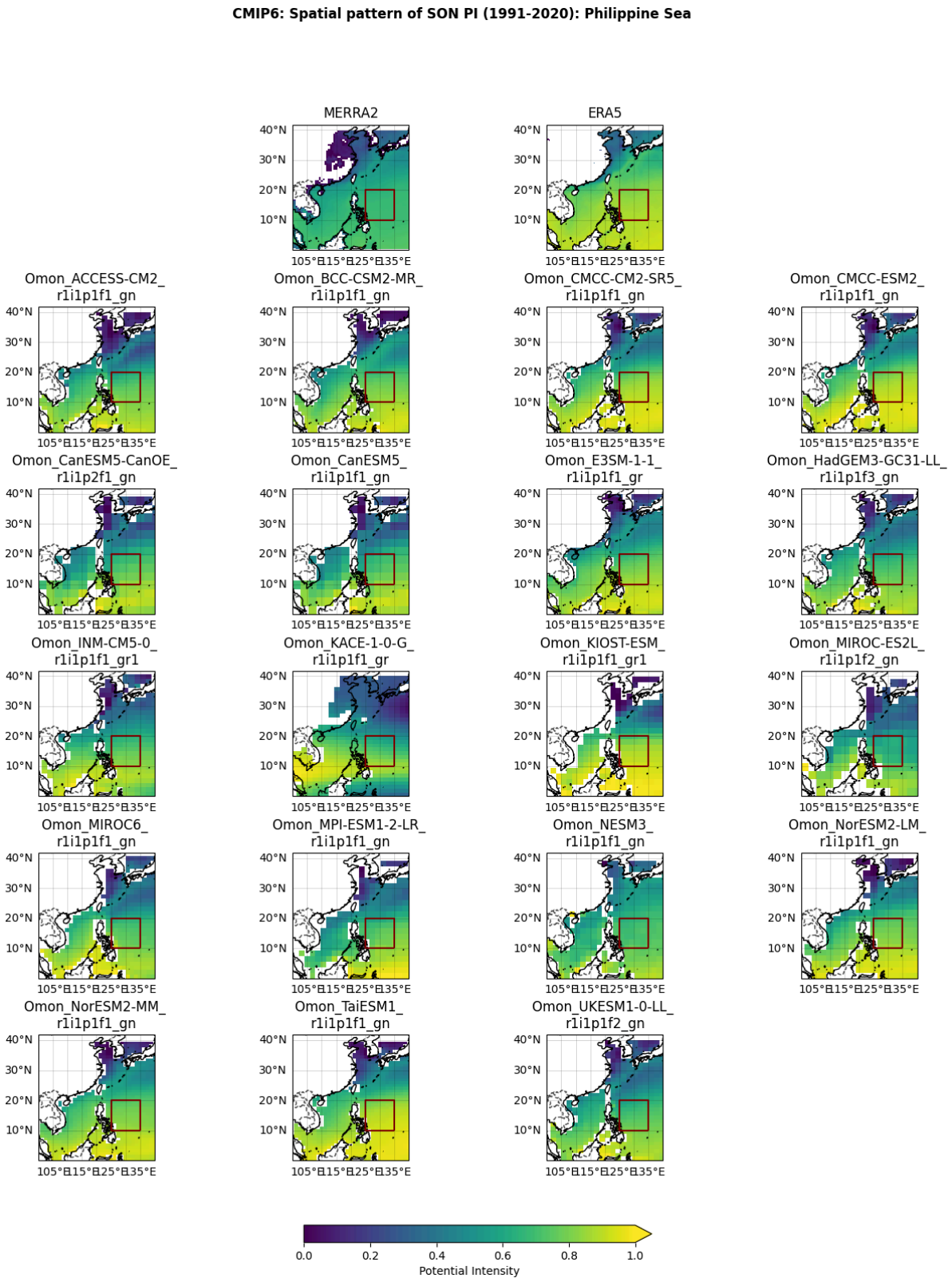

Figure A.1: *Spatial patterns of the standardised average Potential Intensity during September-November in observations and CMIP6 models. The study region for the rainfall analysis is highlighted in red.*

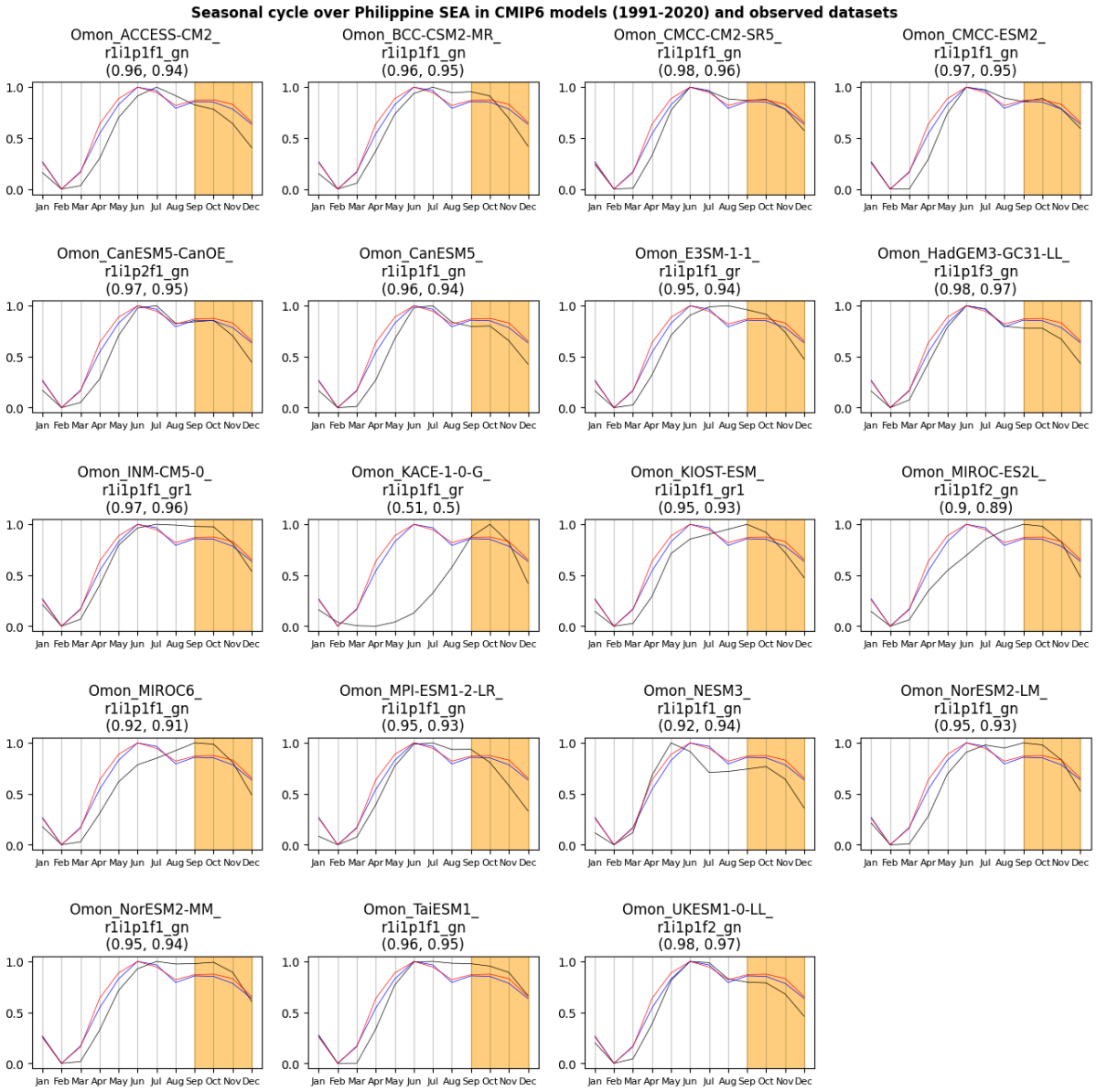

Figure A.2: *Seasonal cycles of the standardised potential intensity in observations and CMIP6. The first number indicates the correlation coefficient of the model with ERA5 (blue) and the second number with MERRA2 (red).*

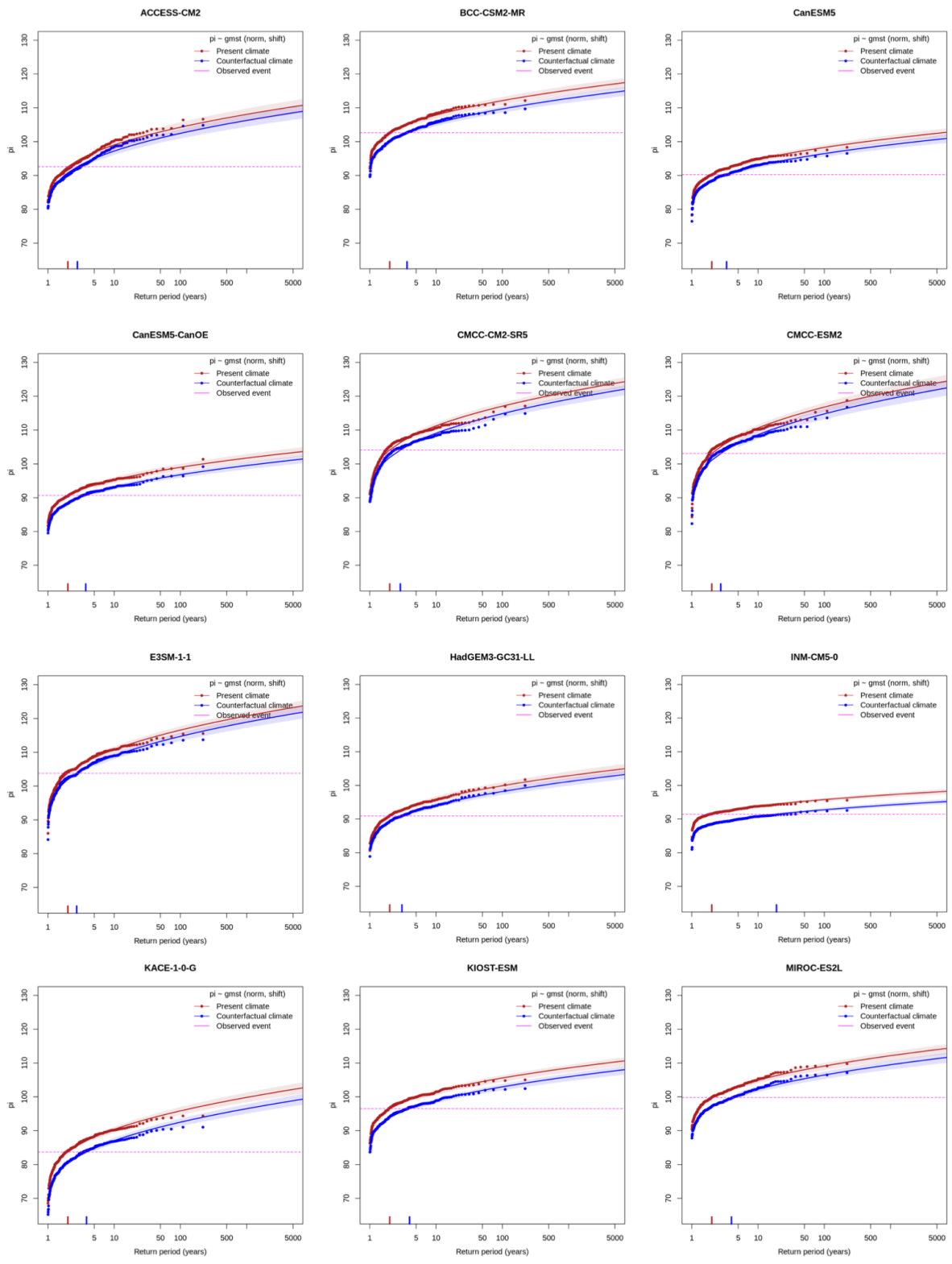

Figure A.3: *Return level plots for CMIP6 models. The influence of GMST is shown in the difference between the red vs blue probability curves and the magnitude of the event is highlighted with a purple line (right). Part 1.*

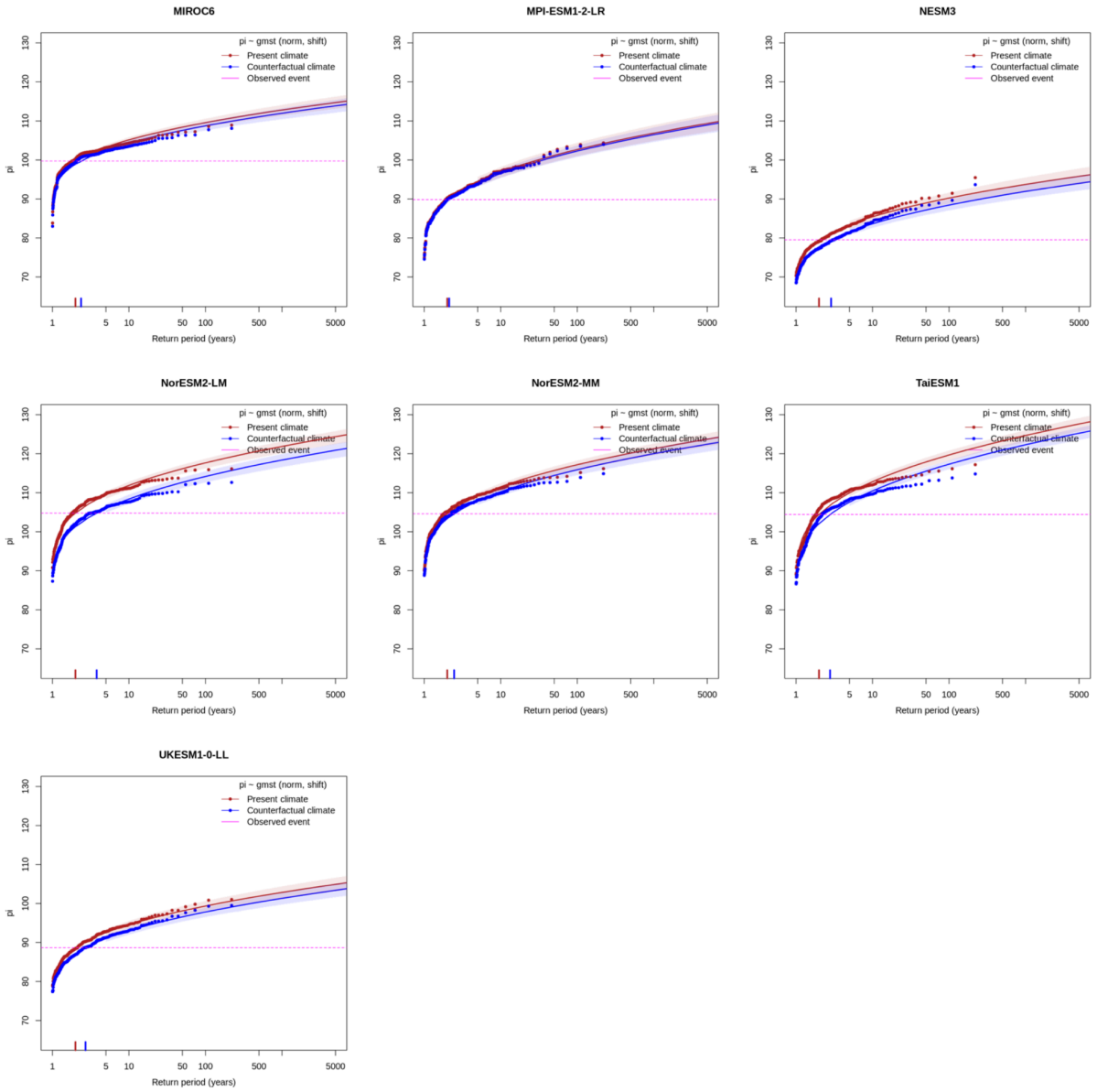

Figure A.3: *Return level plots for CMIP6 models. The influence of GMST is shown in the difference between the red vs blue probability curves and the magnitude of the event is highlighted with a purple line (right). Part 2.*

A.3 Interpreting synthesis figures

Synthesis plots present the estimated changes in intensity or likelihood of the event of interest from both observational datasets (shown as blue bars) and climate models (red bars), along with weighted and unweighted averages of this information that is used to give an overarching attribution statement. The best estimate for each dataset is marked with a black triangle, while the coloured bars represent a 95% confidence interval obtained by bootstrapping. When more than one observational data product is used, a term to account for the spread of the best estimates is added in quadrature to the natural variability of each dataset: this is shown in the figures as a white box around the light blue bars. The dark blue bar indicates the average of the observational data products, including this additional uncertainty. Similarly, a term to account for intermodel spread is added in quadrature to the natural variability of the models: this is shown in the figures as white boxes around the light red bars. The

dark red bar shows the weighted model average, where the weights are derived from the precision (inverse of the variance) of each model estimate.

Observation-based products and models are combined into a single result in two ways - a detailed description including the mathematical formulations can be found in the literature (Philip et al., 2020; Li & Otto, 2022). Firstly, we neglect common model uncertainties beyond the intermodel spread already incorporated in the observational and model averages, and compute the precision-weighted average of models (dark red bar) and observations (dark blue bar): this weighted mean is indicated by the magenta bar. To account for the fact that, due to common model biases, model uncertainty can be larger than the intermodel spread, we also show an unweighted average of the synthesised observations (dark blue bar) and models (dark red bar), indicated by the white box in the bottom row of the synthesis figures.

A.4 Major typhoons landfall rate

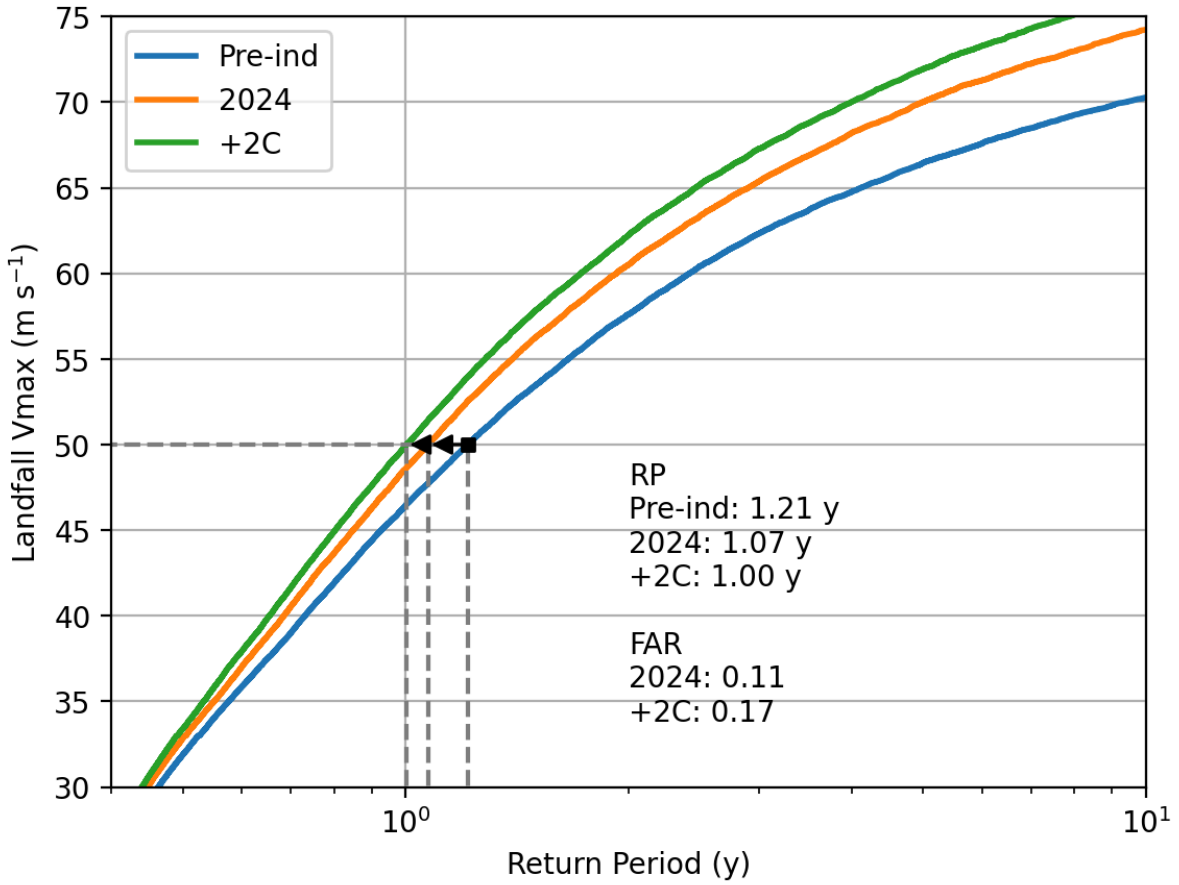

Figure A.4: *The return curves for landfalling typhoons in the Philippines in a given year at different global temperatures: preindustrial, current 2024 conditions, and a world 2 degrees above pre industrial temperatures. The return period of category 3 storms and above are indicated with the dashed lines for each scenario.*